Structural and magnetic properties of $CuCr_{1-x}Mg_xO_2$ by neutron powder diffraction

Maria Poienar,[1] Françoise Damay,[2,*] Christine Martin,[1] Vincent Hardy,[1] Antoine Maignan,[1] and Gilles André[2]
[1]*Laboratoire CRISMAT, ENSICAEN, UMR 6508 CNRS, 6 Boulevard du Maréchal Juin, 14050 Caen Cedex, France*
[2]*Laboratoire Léon Brillouin, CEA-CNRS, UMR12, CEA-Saclay, 91191 Gif-sur-Yvette Cedex, France*
(Received 22 October 2008; revised manuscript received 28 November 2008; published 12 January 2009)

Delafossite antiferromagnetic oxide $CuCrO_2$ was investigated by means of neutron powder diffraction versus temperature. Evolution of the structural parameters (in the $R\bar{3}m$ hexagonal setting) shows a steady decrease in the a lattice parameter but negative thermal expansion along c as the temperature decreases from 300 to 1.5 K. Below $T_N=24$ K, both a and c become constant and a relaxation of the rhombohedral distortion of the CrO_6 octahedra is observed. The magnetic structure of $CuCrO_2$ is noncommensurate and shows a short magnetic correlation length of about 200 Å along c. Symmetry analysis considerations allow us to propose two possible magnetic structures, helicoidal or cycloidal, compatible with ferroelectric properties. Despite having a strong impact on transport and magnetic properties, Mg doping affects only slightly the crystal and magnetic structures, as shown in $CuCr_{0.98}Mg_{0.02}O_2$.

DOI: 10.1103/PhysRevB.79.014412 PACS number(s): 75.25.+z, 75.80.+q, 61.05.F−

I. INTRODUCTION

Layered 3*d* metal delafossite oxides have long been studied for their variety of interesting properties, in particular, transparency with *p*-type conductivity, as observed in thin films of $CuAlO_2$.[1] Recently, the discovery of spin-driven multiferroicity in the layered delafossite compound $CuFeO_2$ (Ref. 2) lead us to study the parent oxide $CuCrO_2$, to which only a few studies had been dedicated. The magnetic properties of $CuCrO_2$ ($T_N \cong 24$ K) were investigated by Doumerc *et al.*[3] in the two-dimensional (2D)-Heisenberg framework. In their pioneer work on the investigation by neutron powder diffraction of the magnetic structure of $CuCrO_2$, Kadowaki *et al.*[4] proposed several possible magnetic models and reported strong magnetic disorder in the stacking *c* direction. Very recently, $CuCrO_2$ was reported to show ferroelectric polarization upon spin ordering,[5] suggesting a strong coupling between ferroelectricity and the assumed 120° spiral structure. Several points remained unclear however; because of the lack of low-temperature structural data, it was not known whether $CuCrO_2$ exhibits a structural phase transition similar to the one observed in $CuFeO_2$ and which could explain the observed three-dimensional (3D) magnetic ordering in a triangular lattice, whose ground state should otherwise stay degenerate.

We therefore decided to perform a neutron-diffraction study versus temperature on $CuCrO_2$ to check for any phase transition and to study the thermal evolution of the crystal and magnetic structures. Symmetry analysis was used to narrow down the number of possible magnetic structures compatible with its ferroelectric properties, and a state-of-the-art Rietveld refinement software was employed to model the magnetic disorder in $CuCrO_2$. The crystal and magnetic structures of $CuCr_{0.98}Mg_{0.02}O_2$, which exhibits significantly different physical properties,[6,7] compared to the undoped compound were also investigated by neutron powder diffraction.

II. EXPERIMENTAL SECTION

$CuCrO_2$ (5 g) was prepared by high-temperature solid-state reaction in air. Powders of Cu_2O and Cr_2O_3 were weighted in the (1:1) stoichiometric ratio, carefully crushed, mixed together, and heated up for several days at 1000 °C with intermediate grindings. The powders were then pressed in the shape of pellets (8 mm diameter and 4 mm thick) and heated up to 1200 °C for 12 h. The quality of the compound was checked by room-temperature x-ray diffraction which confirmed that the sample is single phase, well crystallized, and exhibits the expected delafossite structure [Fig. 1(a)]. The magnetic properties were also measured in 0.3 T while warming from 1.5 to 300 K, after a zero-field cooling, using a Quantum Design superconducting quantum interference device (SQUID) magnetometer. The shape of the susceptibility and inverse susceptibility curves [Fig. 1(b)] and the extracted characteristic parameters—the Néel temperature $T_N \cong 24$ K and the Curie-Weiss temperature $\theta_{CW} \cong -202$ K—are in agreement with literature results.[3,5] The effective moment $\mu_{eff} \cong 3.89\mu_B$ is very close to the theoretical value of $3.87\mu_B$ for Cr^{+3}. Heat-capacity measurements were carried out by means of a commercial physical properties measurements system (PPMS, Quantum Design) using a relaxation method with a 2τ fitting procedure. Neutron powder diffraction versus temperature was performed on the G4.1 diffractometer ($\lambda=2.428$ Å) from 1.5 to 300 K and high-resolution neutron diffractograms were recorded on the diffractometer 3T2 ($\lambda=1.225$ Å) at 300, 100, and 10 K. Both diffractometers are located at LLB, CEA-Saclay, France. Neutron powder diffraction in a magnetic field up to 6 T was performed on the D2B diffractometer ($\lambda=2.398$ Å) at ILL Grenoble (France). Rietveld refinements of the powder diffractograms were performed with the FULLPROF program from the FULLPROF suite,[8] which also includes the BASIREPS program that was used for the representational analysis of the magnetic structures.

$CuCr_{0.98}Mg_{0.02}O_2$ was prepared following the same process, in order to check the impact of substitution upon the magnetic structure. Powder neutron-diffraction data were collected on G4.1 from 1.5 to 50 K and on 3T2 at room temperature. The transport and magnetic properties of this sample are in perfect agreement with those previously reported.[6,7]

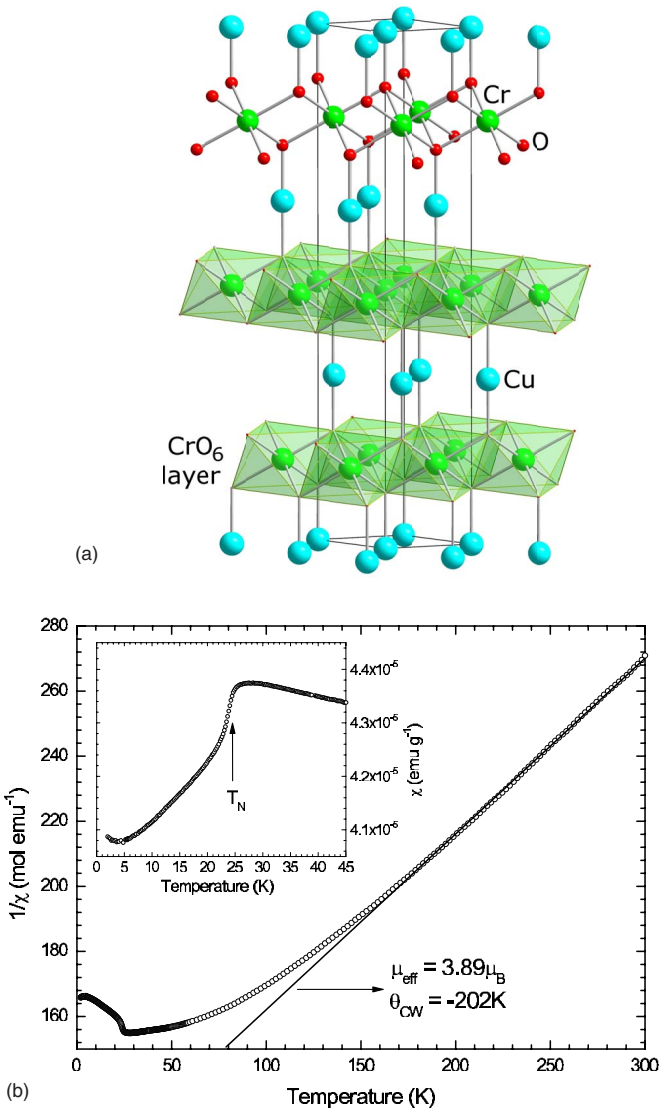

FIG. 1. (Color online) (a) Illustration of the delafossite structure, showing CrO_6 octahedra layers linked through O-Cu-O dumbbells. (b) Evolution with temperature of the inverse susceptibility of $CuCrO_2$ in 0.3 T. The line corresponds to a Curie-Weiss law fit in the paramagnetic state. Inset: enlargement in the T_N vicinity of the susceptibility vs T curve.

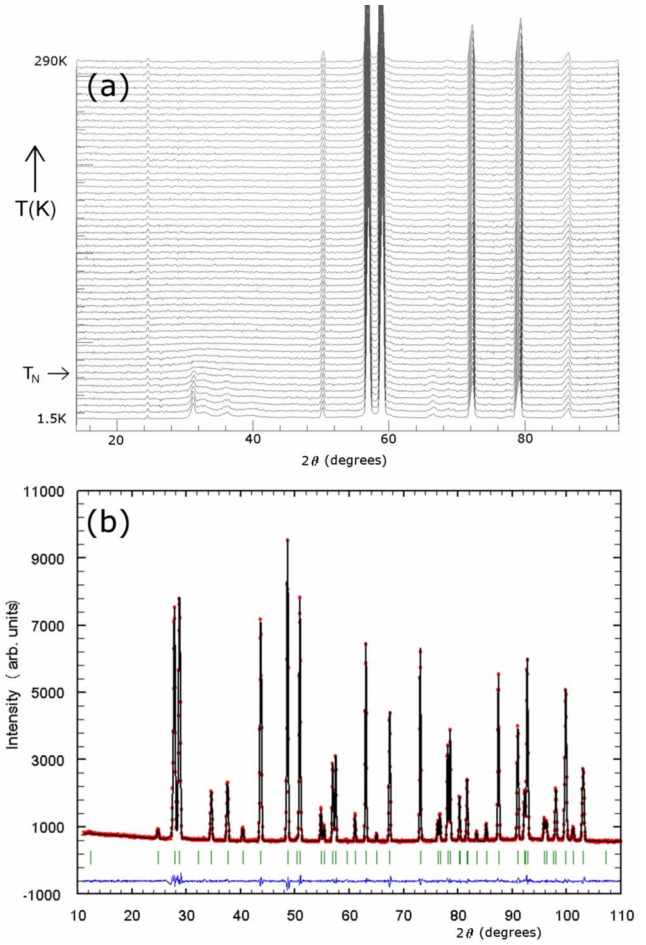

FIG. 2. (Color online) (a) Evolution between 1.5 and 300 K of the neutron diffractograms recorded on $CuCrO_2$ using the G4.1 diffractometer ($\lambda = 2.428$ Å). (b) Refinement of the 300 K neutron-diffraction data of $CuCrO_2$ recorded using the 3T2 diffractometer ($\lambda = 1.225$ Å) (experimental data: open circles; calculated profile: continuous line; and allowed Bragg reflections: vertical marks. The difference between the experimental and calculated profiles is displayed at the bottom of the graph).

III. RESULTS AND DISCUSSION

A. Neutron-diffraction experiments: Crystal structure

$CuCrO_2$ crystallizes in the well-known delafossite structure [$R\bar{3}m$ space group, $a = 2.9760(1)$ Å and $c = 17.1104(6)$ Å at room temperature (RT), in the hexagonal setting], which can be simply described as a stacking of compact layers of CrO_6 octahedra sharing edges, i.e., CdI_2 type, linked through Cu^+ ions linearly coordinated to two oxygen ions [Fig. 1(a)].

The temperature dependence of the neutron diffractograms [Fig. 2(a)] between RT and 1.5 K shows no structural transition, within the instrumental resolution, in this temperature range. The onset of broad magnetic peaks is observed around $\cong 24$ K [see horizontal arrow in Fig. 2(a)], in agreement with the magnetic transition temperature T_N observed in the susceptibility curve reported in Fig. 1(b). These magnetic peaks will be described in more details in Sec. III B.

Evolution of cell parameters a and c and cell volume V with temperature are illustrated in Figs. 3 and 4. In contrast to a, c increases regularly with decreasing T down to T_N. Below T_N, a and c become nearly constant, with $a = 2.9685(1)$ Å and $c = 17.1380(8)$ Å at 10 K. The cell volume V decreases accordingly with decreasing T and becomes roughly constant for $T < T_N$, with $\Delta V/V = 0.38\%$ between RT and 10 K (Fig. 4).

Rietveld refinements were performed on the high-resolution patterns recorded at RT, 100, and 10 K. The quality of the refinements of the crystal structures is very good, as illustrated in Fig. 2(b), for the RT data. Basic structural parameters are reported in Table I, along with the refinement agreement factors. Equivalent isotropic displacement values U do not exceed 4.3×10^{-3} Å^2 for oxygen and 8.5×10^{-3} Å^2 for copper at 300 K; it is therefore reasonable to

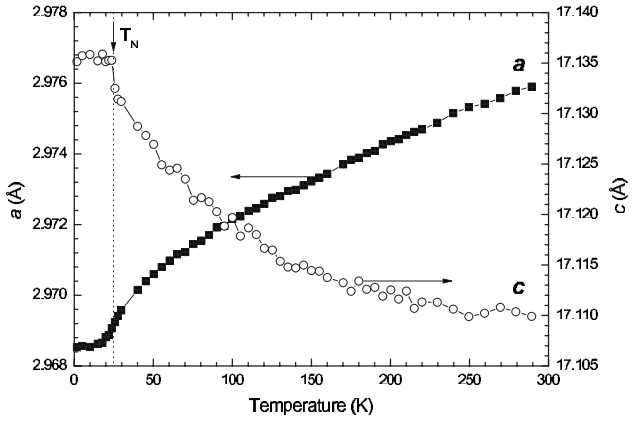

FIG. 3. Temperature evolution of the a and c lattice parameters of $CuCrO_2$ ($R\bar{3}m$, hexagonal setting).

assume accordingly that oxygen nonstoichiometry or ionic disorder is negligible. Anisotropic displacement factors are also reported in Table I: U_{11} and U_{33} are perpendicular and parallel to the c axis, respectively, and define the displacement ellipsoids either flattened or elongated along c. The values listed in Table I show that Cu^+ has the largest isotropic $U=8.5\times10^{-3}$ Å^2 ($B_{eq}\cong0.67$ Å^2) and the largest U_{11} ($>U_{33}$) corresponding to a flattened ellipsoid along c. Such flattened ellipsoids are often encountered in twofold linear coordination and are described as resulting from transverse "guitar string" vibration.[9] The chromium ions in their octahedral environment have the smallest isotropic displacements factors, in agreement with the fact that the CrO_6 octahedra layers are close compact. In addition, contrary to Cu^+, the displacement ellipsoid is slightly elongated along c, that is, in the direction of the octahedron's two larger faces [which are delimited by three distances (O-O_{in}), the four remaining faces being defined by one distance (O-O_{in}) and two smaller distances (O-O_{out}), see Table II and text below], in connection with the distorted nature of the octahedra.[10]

The refined lattice parameters obtained from the 3T2 data at 100 and 10 K confirm the temperature dependence obtained from G4.1 measurements. Corresponding selected

TABLE I. Rietveld refinement results of high-resolution neutron powder diffractograms of $CuCrO_2$ at 300, 100, and 10 K [space group $R\bar{3}m$ ($n°166$, H setting) with Cu in $3a$ (0, 0, 0), Cr in $3b$ (0, 0, 0.5), and O in $6c$ $(0,0,z)$].

Temperature	300 (K)	100 (K)	10 (K)
Cell parameters (Å)			
a	2.9760(1)	2.9719(1)	2.9685(1)
c	17.1104(6)	17.1198(7)	17.1380(8)
Cell volume V (Å^3)	131.2(1)	130.9(1)	130.8(1)
Oz	0.10788(2)	0.10785(2)	0.10775(2)
$U_{isotropic}$ (10^{-3} Å^2)			
Cu	8.5(2)	3.2(2)	1.8(1)
Cr	3.3(1)	1.5(1)	0.8(1)
O	4.3(2)	2.4(2)	2.0(2)
$U_{anisotropic}$ (10^{-3} Å^2)			
CuU_{11}	6.61(9)	2.56(8)	1.50(9)
CuU_{33}	3.6(3)	1.0(3)	0.5(3)
CrU_{11}	1.48(12)	0.63(11)	0.48(14)
CrU_{33}	4.9(4)	2.4(4)	0.8(5)
OU_{11}	2.91(7)	1.70(7)	1.51(8)
OU_{33}	3.2(2)	1.5(3)	1.0(3)
No. of reflections	75	75	73
No. of parameters	17	17	17
Bragg R factor	1.29	1.74	1.60
χ^2	2.97	3.86	6.90

atomic distances and angles are listed in Table II. Despite the increase in the c parameter with decreasing temperature, the Cu-O distance stays approximately constant between 300 and 10 K (about 1.846 Å). This observation contrasts with what has been reported for several nonmagnetic delafossite (Ag,Cu)MO_2 compounds (with M=Al, In, La, and Sc),[10] for which the negative thermal expansion (NTE) along c is attributed to an increasing Cu-O distance as T decreases, related to the softening of the vibration mode perpendicular to

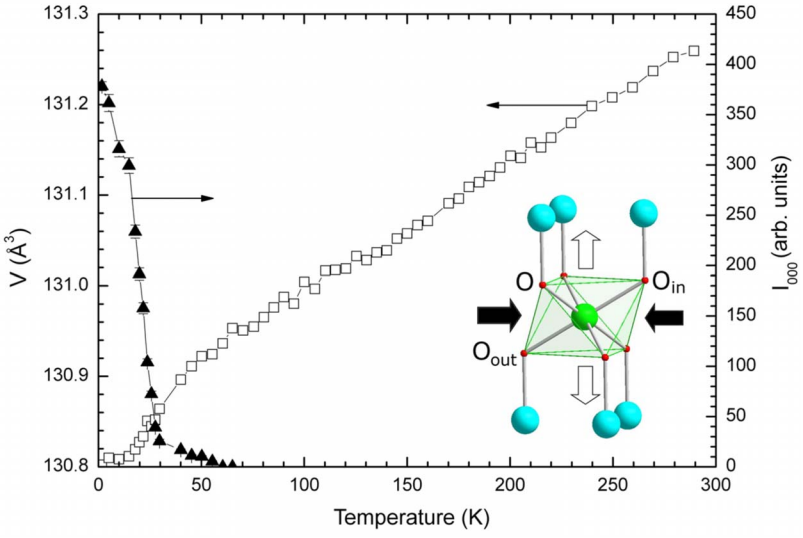

FIG. 4. (Color online) Temperature evolution of the cell volume V and of the intensity of the (0 0 0) magnetic peak extracted from the G4.1 neutron diffractograms for $CuCrO_2$. Inset: Illustration of the deformation of the CrO_6 octahedra below T_N.

TABLE II. Selected interatomic distances and angles in $CuCrO_2$ at 300, 100, and 10 K (from high-resolution neutron powder diffractograms).

Temperature	300 (K)	100 (K)	10 (K)
	Distances (Å)		
Cu-O	1.8459(3)	1.8464(4)	1.8463(4)
Cr-O	1.9910(2)	1.9895(2)	1.9894(2)
$Cr\text{-}Cr_{in}$	2.9760(1)	2.9718(1)	2.9685(1)
$Cr\text{-}Cr_{out}$	5.9567(2)	5.9590(2)	5.9642(3)
$Cr\text{-}Cr_{in}$ (second neighbor)	5.1546(2)	5.1475(1)	5.1416(2)
$(O\text{-}O_{in})$	2.9760(1)	2.9719(1)	2.9685(1)
$(O\text{-}O_{out})$	2.6456(4)	2.6457(4)	2.6492(4)
$(O\text{-}O_{in})/(O\text{-}O_{out})$	1.1249(3)	1.1233(3)	1.1205(3)
CrO_2 layer thickness (Å)	2.0117(3)	2.0139(4)	2.0201(4)
	Angles (deg)		
$O\text{-}Cr\text{-}O_{in}$	96.727(8)	96.647(9)	96.507(9)
$O\text{-}Cr\text{-}O_{out}$	83.273(8)	83.353(8)	83.494(9)
Cu-O-Cr	120.345(11)	120.406(11)	120.513(11)
Cr-O-Cr	96.727(9)	96.647(9)	96.507(9)

the O-Cu-O linkage. The guitar string vibration, however, does not necessarily imply a shortening of the Cu-O bond but rather a departure from the linear O-Cu-O bond and a shortening of the O-O distance. The oxygen thermal displacement ellipsoids are slightly elongated along c. In the series studied by Li *et al.*,[10] the $[MO_2]_\infty$ layer thickness decreases with decreasing temperature. In $CuCrO_2$, however, the $[CrO_2]_\infty$ layers themselves show NTE behavior, i.e., there is a marked increase in the thickness of the $[CrO_2]_\infty$ layers given by $(1/3-2z_O)c$ from 2.0117(3) Å at 300 K up to 2.0201(4) Å at 10 K, as the Cr-O distances within the CrO_6 octahedron decrease.

In the delafossite structure, the CrO_6 octahedron is slightly compressed along the threefold axis (D_{3d} symmetry), even though the six Cr-O distances are equal because the O-Cr-O angles depart from 90°. To estimate the degree of deformation of the octahedron, it is convenient to use the ratio $(O\text{-}O_{in})/(O\text{-}O_{out})$ defined by Doumerc *et al.*,[11] where $(O\text{-}O_{in})$ is the distance between two oxygen atoms of a CrO_6 octahedron edge parallel to the (a,b) plane of the hexagonal plane [that is, $(O\text{-}O_{in})=a$] and $(O\text{-}O_{out})$ is the length of the octahedron edge delimited by the two oxygen atoms belonging to the two successive oxygen planes on each side of the Cr^{+3} layer (inset of Fig. 4). Between 300 and 10 K, the Cr-O distances decrease from 1.9910(2) to 1.9894(2) Å, the $(O\text{-}O_{in})/(O\text{-}O_{out})$ ratio decreases from 1.1249(3) to 1.1205(3), and the Cr-O-Cr angle decreases simultaneously from 96.727(9)° to 96.507(9)°, implying a relaxation of the compression along c of the CrO_6 octahedron (this effect is schematized by the arrows in the inset of Fig. 4). A similar "regularization" of the CrO_6 octahedra has been observed by Doumerc *et al.*[11] in AMO_2 delafossites (A=Cu or Ag and M=Co, Ti, Ni, Sn, and Sc) when decreasing the size in the M cation and was interpreted as an increase in the M-O bond covalence. Because we are dealing here with a magnetic material, however, it is likely that the observed structural evolution is related to the ordering of the spins below T_N, as will be discussed later.

TABLE III. BV of the irreducible representation and corepresentation of space group $R\bar{3}m$ with $k=(2q,-q,0)$ (q=0.329). Magnetic moment for an atom j is given by $m_j=\Sigma_i C_i\psi_i$, where C_i's are the mixing coefficients of the BVs.

IR	BV	BV real part components		
$\Gamma_1(\Delta_1)$	$\psi_1(\phi_1)$	1	0	0
$\Gamma_2(\Delta_2)$	$\psi_1'(\phi_1')$	1	2	0
	$\psi_2'(\phi_2')$	0	0	1

B. Neutron-diffraction experiments: Magnetic structure

Around $T_N \cong 24$ K, broad and overlapped magnetic peaks appear [Figs. 2(a) and 4]. They can be indexed with an incommensurate propagation vector $k=(2q,-q,0)$ labeled k_2 in Kovalev's notation.[12] Two one-dimensional irreducible representations (IRs) are associated with the $R\bar{3}m$ space group and $k=(2q,-q,0)$ for the Cr site (0, 0, 0.5). The magnetic representation can be decomposed as $\Gamma_{mag}=1\Gamma_1\oplus 2\Gamma_2$; the corresponding basis vectors (BVs) being listed in Table III. Only representation Γ_2 (with the two modes ψ_1' and ψ_2') or the mixture $\Gamma_1\oplus 2\Gamma_2$ (with three modes ψ_1, ψ_1', and ψ_2') can fit the experimental data. In this framework, representational analysis was extended to the use of corepresentations[13] to determine the magnetic point groups of the different possible magnetic structures. Accordingly, there are four symmetry operations in the little corepresentation group and two one-dimensional corepresentations, whose characters are listed in Table IV. The magnetic corepresentation Δ_{mag} is decomposed into $\Delta_1\oplus 2\Delta_2$ and its basis vectors are given in Table III. Among the seven possible linear combinations of basis vectors, three lead to magnetic structures with polar point groups, which are schematized in Fig. 5(a). The first one (i) is obtained by mixing two modes belonging to Δ_2 ($\phi_1'+i\phi_2'$) and describes a helicoidal modulation with an elliptical envelope. In this case the point group is 2 (magnetic point group 2′) and ferroelectricity is therefore possible along a [as illustrated on Fig. 5(a) by the big arrow noted **P**]. Two other magnetic structures can be obtained by mixing

TABLE IV. Corepresentations of space group $R\bar{3}m$ for propagation vector $k=(2q,-q,0)$ (q=0.329). The magnetic atom is Cr (0, 0, 0.5). The symmetry operators are in the Kovalev notation and correspond to the international tables symbols: $h_1\equiv 1$; $h_9\equiv 2x,0,0$; $h_{13}\equiv \bar{1}0,0,0$; and $h_{24}\equiv m2x,x,z$.

	h_1	h_9	Kh_{13}	Kh_{24}
Δ_1	1	1	1	1
Δ_2	1	−1	1	−1

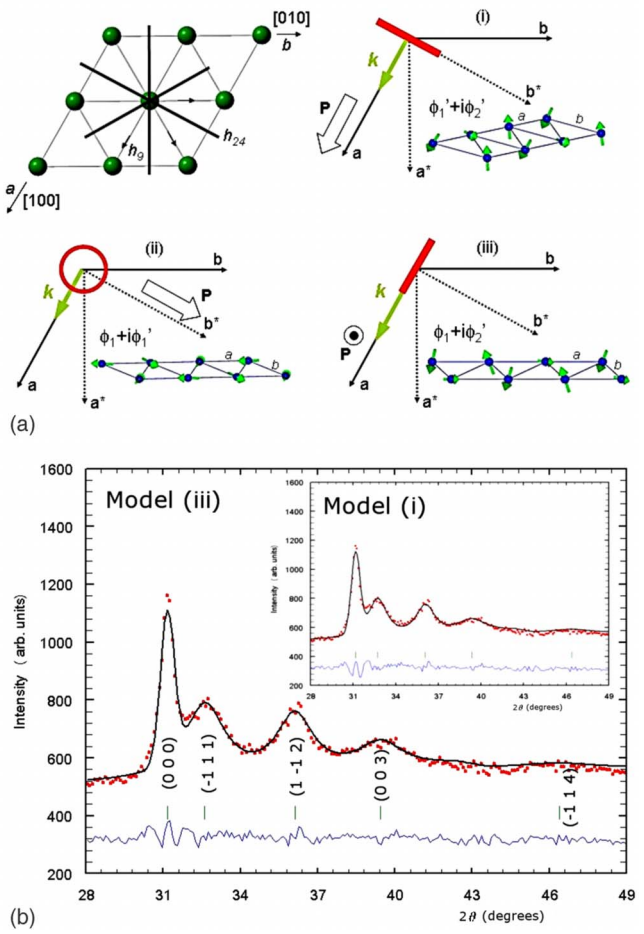

FIG. 5. (Color online) (a) Projection in the (a,b) plane of the symmetry elements in the little corepresentation group $[R\bar{3}m,\ k=(2q,-q,0)]$ and corresponding schematic drawings of the three possible magnetic structures (i), (ii), and (iii) derived from corepresentation analysis (see text). For each case, the magnetic propagation vector (k) is given, the spin rotation plane is shown as a thick bar (red online) in (i) and (iii), or as a circle in (ii), and the large arrow indicates the expected direction of the polarization (**P**). (b) Refinement of the magnetic peaks of $CuCrO_2$ at 1.5 K (G4.1 neutron powder diffractogram) for the cycloidal magnetic structure model (iii). Peaks indexation corresponds to the magnetic propagation vector k. Inset: Refinement using the helicoidal magnetic structure model (i).

modes belonging to Δ_1 and Δ_2: (ii) $(\phi_1+i\phi_1')$ and (iii) $(\phi_1+i\phi_2')$. The point group in this case is m and the magnetic point group is also m. These magnetic structures correspond to cycloids with elliptic modulation, which can both give rise to ferroelectricity [along b^* for (ii) and along c for (iii)] in the framework of the microscopic spin current model.

To account for the short-range magnetic correlations evidenced by the broad magnetic peaks, a model of plateletlike-shaped magnetic crystallites disorderly stacked along c [size model=1 in FULLPROF (Ref. 8)] was applied for both the helicoidal and cycloidal structures. This model corresponds to a finite spin-correlation length in the c direction, with long-range magnetic order being established in the (a,b) plane. The refinement was further improved by introducing anisotropic shifts on the magnetic peaks position, likewise to anisotropic shifts resulting from stacking faults in a crystal structure; it is however important to emphasize here that there is no abnormal broadening (within the instrumental resolution) of the *crystal* structure peaks and that, therefore, the short-range magnetic correlations observed in $CuCrO_2$ do not result from structural defects such as stacking faults along c.

This model gives a very satisfactory fit to the experimental data, as illustrated on Fig. 5(b), with a magnetic Bragg factor $R=12.7\%$ for the helicoidal structure [model (i)] and 9.9% for the cycloidal one [model (iii)]. It is not possible, however, to distinguish unambiguously between models (i) and (iii) with the powder-diffraction data only. Even though the magnetic R_{Bragg} factor is better for the cycloidal structure, it is not enough so to decide convincingly that this model is the correct one. Because of the short-range magnetic correlations, the lower magnetic R_{Bragg} value could just be the result of a slightly better fit of the peak shape unrelated to the intrinsic magnetic structure. Rietveld refinements also show quite clearly that the cycloidal structure (ii), in which spins are all within the (a,b) plane, leads to quite poorer agreements factors ($R_{\mathrm{Bragg}}=24.2\%$) than models (i) and (iii), in which spins can have a component along c. This also correlates well with the low-temperature structural behavior that is observed: at the onset of magnetic ordering, the crystal structure constricts in the (a,b) plane but expands in the NTE c direction, as could be expected with models (i) and (iii), in contrast to model (ii), which should rather lead to an expansion of the structure in the (a,b) plane.[14]

For both magnetic structures (i) and (iii), the maximum moment on a Cr^{+3} site is $\cong 2.9(2)\mu_B$ and the magnetic correlation length along c is found to be close to 200 Å. Both models are in fact not dissimilar since they have a main spin component along c, the only difference being the spin rotation plane. These two types of magnetic structures obtained here with corepresentation theory are in agreement with those recently suggested in Ref. 5, using the 120° model of Kadowaki *et al.*[4]

To go further in the understanding of the magnetic properties of Cu-based delafossites, a similar study was undertaken on $CuCr_{0.98}Mg_{0.02}O_2$. In fact, substituting nonmagnetic Mg^{+2} for Cr^{+3} in $CuCrO_2$ is known to dramatically decrease the resistivity and to sharpen the antiferromagnetic transition at T_N.[7,15] The effect of 2% Mg for Cr substitution is illustrated in Figs. 6(a) and 6(b). In agreement with previous results,[7,15] Mg substitution induces a less resistive electrical behavior [inset (b) of Fig. 6(a)], which corresponds to a decrease in the Seebeck coefficient from $\cong 1100$ to 230 $\mu V\ K^{-1}$ at 300 K (not shown). The peaks observed in the specific-heat curves around T_N [Fig. 6(a)] indicate the 3D long-range character of the magnetic order (in contrast to a true 2D Heisenberg system) in both $CuCrO_2$ and $CuCr_{0.98}Mg_{0.02}O_2$ compounds. The $C/T(T^2)$ curves [inset (a) of Fig. 6(a)] are linear for both compounds, with $\gamma\cong 0$ (<1 mJ/K^2 mol), in agreement with previous measurements.[15] There is thus no electronic contribution—lattice and antiferromagnetism contributions only—to the specific heat. This is in agreement with the absence of density of state (DOS) at the Fermi level, as calculated in Ref.

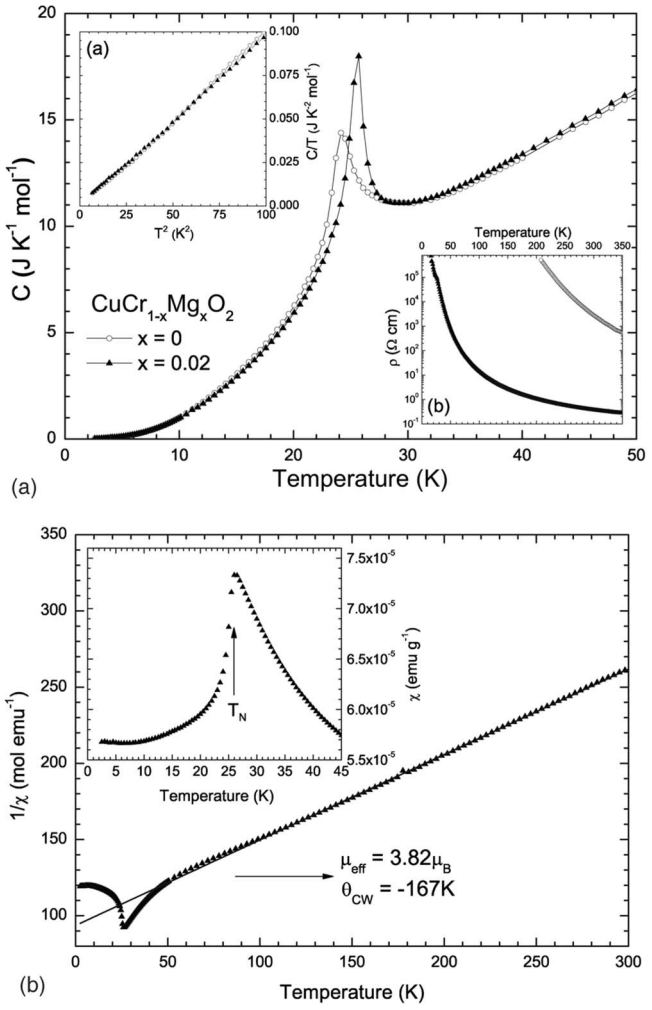

FIG. 6. (a) Variation with temperature in the specific-heat C in the vicinity of T_N for $CuCr_{1-x}Mg_xO_2$ ($x=0,0.02$). Insets: (a) $C/T(T^2)$ and (b) resistivity $\rho(T)$ for $x=0$ and $x=0.02$. (b) Evolution with temperature of the inverse susceptibility in 0.3 T of $CuCr_{0.98}Mg_{0.02}O_2$. The line corresponds to a Curie-Weiss law fit in the paramagnetic state. Inset: Enlargement in the T_N vicinity of the susceptibility vs T curve.

16. A small increase in T_N from 24 to 25.5 K upon substitution is also visible in Fig. 6(a), in agreement with the transition temperatures determined from the susceptibility curves [Figs. 1(b) and 6(b)]. Moreover the transition is sharper for the doped sample, indicating an enhancement of the 3D character, in agreement with the magnetic peak profiles (Fig. 7). This could be explained by a partial lifting of the frustration of the triangular lattice (due to the doping-induced dilution) or by an increase in the interlayer coupling.

To investigate structural changes upon substitution, high-resolution neutron diffraction was performed at room temperature on $CuCr_{0.98}Mg_{0.02}O_2$ (Table V). Within the accuracy of the technique, no cationic nor oxygen deficiency was detectable, in spite of about 1% in weight of $MgCr_2O_4$ spinel impurity being detected by x-ray diffraction. Owing to the neutron-scattering factor of Mg, intermediate between those of Cr and Cu, no information can be obtained on the location and amount of Mg on 3*a* or 3*b* sites. Anisotropic displacement factors in the doped sample are similar to those of $CuCrO_2$, with in particular Cu^+, exhibiting also a flattened ellipsoid along *c*. Refinement results show a slight contraction of the *a* and mostly *c* parameters and a consequent decrease in the Cr-Cr_{in} and Cr-Cr_{out} distances (Table V) upon substitution. The contraction of the CrO_6 octahedra is slightly larger [$(O\text{-}O_{in})/(O\text{-}O_{out})=1.1255(5)$ to be compared with 1.1249(3) in $CuCrO_2$] because of a decrease in the ($O\text{-}O_{out}$) distance [from 2.6456(4) Å in $CuCrO_2$ to 2.6435(6) Å in the 2% Mg-doped compound]. The CrO_2 layer thickness decreases accordingly from 2.0117(3) Å in

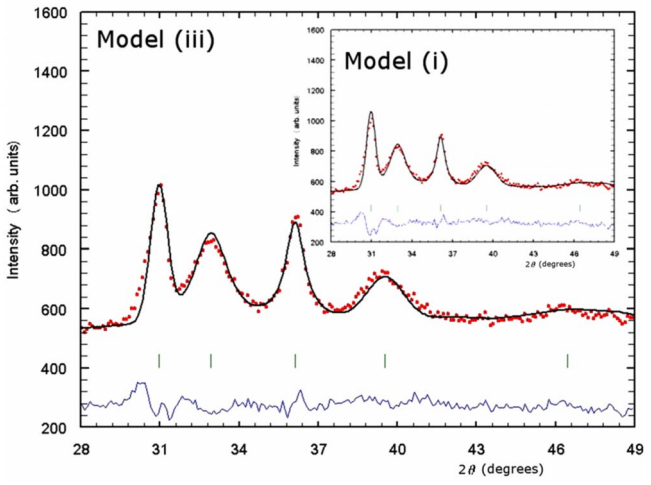

FIG. 7. (Color online) Refinement of the magnetic peaks of $CuCr_{0.98}Mg_{0.02}O_2$ at 1.5 K (G4.1 neutron powder diffractogram) for the cycloidal magnetic structure model (iii). Inset: refinement using the helicoidal magnetic structure model (i).

TABLE V. Rietveld refinement results of the 300 K high-resolution neutron powder diffractograms of $CuCr_{0.98}Mg_{0.02}O_2$ [in $R\bar{3}m$ ($n°$166, H setting) with Cu in 3*a* (0, 0, 0); Cr, Mg in 3*b* (0, 0, 0.5); and O in 6*c* $(0,0,z)$], and corresponding selected interatomic distances and angles (in Å and in deg).

Cell parameters (Å)			
a	2.9752(1)	No. of reflections	74
c	17.0931(7)	No. of parameters	17
Cell volume V (Å^3)	131.0(1)	$U_{isotropic}(10^{-3}$ Å$^2)$	
O *z*	0.10789(2)	Cu	8.6(2)
Bragg *R* factor	0.60	Cr/Mg	2.7(1)
χ^2	2.21	O	3.7(2)
Cu-O	1.8442(5)	$(O\text{-}O_{in})$	2.9752(1)
Cr-O	1.9900(3)	$(O\text{-}O_{out})$	2.6435(6)
Cr-Cr_{in}	2.9752(1)	$(O\text{-}O_{in})/(O\text{-}O_{out})$	1.1255(5)
Cr-Cr_{out}	5.9510(2)		
Cr-Cr_{in} (second neighbor)	5.1532(1)	CrO_2 layer thickness (Å)	2.0094(5)
O-Cr-O_{in}	96.757(12)	Cu-O-Cr	120.323(16)
O-Cr-O_{out}	83.243(12)	Cr-O-Cr	96.757(13)

$CuCrO_2$ to 2.0094(5) Å in $CuCr_{0.98}Mg_{0.02}O_2$. The Cu-O distance is also smaller in the doped sample [1.8459(3) Å in $CuCrO_2$ to be compared with 1.8442(5) Å in $CuCr_{0.98}Mg_{0.02}O_2$]. The changes reported here are subtle and bordering the accuracy of the technique; they should therefore be interpreted with care: they most probably reflect a global trend, the decrease in a and c upon substitution and the consequent decrease in the distances in the structure.

It is clear, however, from our neutron powder-diffraction study that the magnetic structure of $CuCr_{0.98}Mg_{0.02}O_2$ does not show any major difference with that of undoped $CuCrO_2$. The two samples exhibit roughly similar neutron-diffraction patterns [see Figs. 5(b) and 7] despite having different susceptibility vs T behaviors [Figs. 1(b) and 6(b)]. As for $CuCrO_2$, broad magnetic peaks are also observed for $CuCr_{0.98}Mg_{0.02}O_2$, with a propagation vector $(2q,-q,0)$ close to that of $CuCrO_2$ [refined to $q=0.326(1)$]. The helicoidal and cycloidal magnetic structures lead to magnetic R_{Bragg} of 11.6% and 10.3%, respectively (Fig. 7), using the same magnetic disorder model as for $CuCrO_2$. Within the accuracy of the neutron powder-diffraction technique, the magnetic moment on Cr^{+3} is comparable to the one observed in $CuCrO_2$, about $3\mu_B$, with a component along c. The shapes of the magnetic peaks, as well as their relative intensities, nevertheless, differ slightly for both compounds. It can be argued indeed that narrower peaks are observed in the doped sample, which would suggest that the disorder observed in $CuCrO_2$ is affected by the substitution, and this should in turn have an impact on the physical properties. The lack of change in the magnetic structure of $CuCrO_2$ upon doping is probably linked to its intrinsic disorder; in contrast, in $CuFeO_2$, doping has been reported to modify drastically the magnetic structure from collinear to helicoidal.[17]

C. Discussion

As shown by the results of this study and in agreement with the previous report of Kadowaki *et al.*,[4] the magnetic behavior of this delafossite compound is complex, probably because of the 2D character of the structure combined with the frustrated antiferromagnetic triangular lattice of the chromium layer. Nevertheless a 3D magnetic order with a short coherence length along c is observed. This short coherence length is intrinsic to the sample and is not sensitive to the application of a magnetic field, at least up to 6 T, as was revealed by a neutron powder-diffraction experiment performed in 6T at 10 K after a 6 T field cooling: with reference to the 0 T profile, no change was observed either on the peak profile or peak intensity after cooling the sample in 6 T.

In terms of magnetic exchange, weak direct Cr^{+3}-Cr^{+3} antiferromagnetic interactions should be considered here, as interactions between octahedral site cations sharing a common edge do not involve an anion intermediary, as pointed out by Goodenough.[17] The decrease in the Cr-Cr distance resulting from the contraction of a with decreasing temperature leads to a Cr-Cr interatomic distance of 2.9685(1) Å at 10 K. It is nevertheless probably necessary to take into account indirect exchanges, as discussed in the following. In that case, the Cr-O-Cr angle value is a parameter of importance and its temperature dependence is described in Sec. III A (Table II). Several Cr-O-O-Cr pathways via $O\text{-}O_{\mathrm{in}}$ and $O\text{-}O_{\mathrm{out}}$ are also conceivable.

Because of the 3D magnetic order, indirect superexchange interactions through O-Cu-O linkages have also to be taken into account. Interlayer coupling is indeed necessary to explain the increase in T_N ($\cong$24 K) compared to the theoretical antiferromagnetic transition temperature calculated to be $T_{\mathrm{KM}}=15.9$ K without interlayer coupling.[4] The evolution of structural parameters shows however two competing effects. On one hand, the Cu-O-Cr angle mediating interlayer superexchange interactions increases between 300 and 10 K, consequently increasing interlayer coupling. On the other hand, the interlayer ($Cr\text{-}Cr_{\mathrm{out}}$) distance increases with decreasing temperature, suggesting a weakening of the coupling between layers. It is possible that this competition results in the strongly disturbed magnetic order which is observed.

No structural transition being evidenced, $CuCrO_2$ is supposed to retain its $R\bar{3}m$ symmetry down to T_N and the degeneracy of the frustrated triangular lattice cannot be lifted through intralayer interactions between chromium ions. This is in sharp contrast with what is observed in $CuFeO_2$, which undergoes a $C2/m$ distortion around 11 K and for which three types of ferromagnetic second-neighbor interactions $Fe\text{-}O\text{-}O\text{-}Fe_{\mathrm{in}}$ are proposed to lift the degeneracy in the basal plane.[18,19] Short-range magnetic interactions become appreciable in $CuCrO_2$ below 100 K, as shown by the broad magnetic diffuse scattering around $2\theta\sim 31°$ on the neutron data (Figs. 2 and 4), and by the departure from linearity of the inverse susceptibility vs T curve [Fig. 1(b)]. In addition, below 100 K, a faster decrease in the a lattice parameter is also noticeable, whereas the increase in c remains constant, which suggests that these short-range magnetic interactions lay mainly in the (a,b) plane.

Up to now, the parameters which govern the multiferroic properties in this compound have not been clearly identified, as discussed in recent papers.[5,20] In the parent compound $CuFeO_2$, ferroelectric polarization in the incommensurate magnetic phase, which is helicoidal with a $(q,q,0)$-type modulation vector, has recently been explained by a variation in the π bonding between the magnetic Fe^{+3} ion and the oxygen ion under spin-orbit coupling (direct exchange between the magnetic ions is not considered in this model, which uses a two-ion Fe-O cluster).[21] Whether this approach is appropriate or not to explain multiferroic properties in $CuCrO_2$ is beyond the scope of this paper; it is possible, however, to find magnetic structure models for $CuCrO_2$ which allow ferroelectricity either in the hexagonal plane [model (i)] or perpendicular to it [model (iii)], according to the above mechanism or to the spin current theory, respectively. Polarization experiments on single crystals of $CuCrO_2$ could be a way to discriminate between models. Indeed, a very recent study by Kimura *et al.*[20] showed that the magnetization-induced electric polarization is measured in the (a,b) plane, in agreement with the helicoidal magnetic structure model (i) proposed here.

IV. CONCLUSION

Delafossite oxides $CuCrO_2$ and $CuCr_{0.98}Mg_{0.02}O_2$ were studied by powder neutron diffraction. Despite exhibiting

different transport and magnetic-susceptibility properties, both compounds show similar magnetic structures with broad magnetic peaks in incommensurate positions, which can be interpreted as 3D magnetic order with a short correlation length along *c*, likely resulting from stacking faults of the magnetic planes in the *c* direction. Symmetry analysis suggests that two types of magnetic structures are possible, either a helicoidal one with the spin rotation axis along *a* or a cycloidal one with the spin rotation axis parallel to [120]. Interestingly, regarding the ferroelectricity, both magnetic structures are compatible with the existence of an electric polarization either along *a* (helicoidal magnetic order) or along the *c* axis (cycloidal magnetic order). In $CuCrO_2$, the onset of magnetic ordering at T_N is accompanied by a relaxation of the compression along *c* of the CrO_6 octahedron resulting from the increase in the CrO_2 layer thickness. In contrast, 2% Mg substitution leads to a decrease in the thickness of the CrO_2 layer at room temperature and to an increase in T_N. The role of each CrO_2 and Cu layer deserves probably more attention; in fact, due to the very limited level of substitution, the location of the Mg^{+2} cations remains an open question and so is the determination of the Cu^{+1}/Cu^{+2}-Cr^{+3}/Cr^{+4} species in the matrix and their exact role on the magnetic and transport properties. Nevertheless, the dilution of the chromium antiferromagnetic lattice (via Mg^{+2} or Cr^{+4}) is likely to be the factor influencing predominantly the magnetic interactions.

ACKNOWLEDGMENT

The authors thank J. Rodriguez-Carvajal and L. Chapon for fruitful discussions and E. Suard for the neutron-diffraction experiment in magnetic field.

*francoise.damay@cea.fr

[1] H. Kawazoe, M. Yasukawa, H. Hyodo, M. Kurita, H. Yanagi, and H. Hosono, Nature (London) **389**, 939 (1997).
[2] T. Kimura, J. C. Lashley, and A. P. Ramirez, Phys. Rev. B **73**, 220401(R) (2006).
[3] J. P. Doumerc, A. Wichainchai, A. Ammar, M. Pouchard, and P. Hagenmuller, Mater. Res. Bull. **21**, 745 (1986).
[4] H. Kadowaki, H. Kikuchi, and Y. Ajiro, J. Phys.: Condens. Matter **2**, 4485 (1990).
[5] S. Seki, Y. Onose, and Y. Tokura, Phys. Rev. Lett. **101**, 067204 (2008).
[6] T. Okuda, N. Jufuku, S. Hidaka, and N. Terada, Phys. Rev. B **72**, 144403 (2005).
[7] T. Okuda, T. Onoe, Y. Beppu, N. Terada, T. Doi, S. Miyasaka, and Y. Tokura, J. Magn. Magn. Mater. **310**, 890 (2007).
[8] J. Rodriguez-Carvajal, Physica B **192**, 55 (1993).
[9] J. S. O. Evans, J. Chem. Soc. Dalton Trans. **19**, 3317 (1999).
[10] J. Li, A. W. Sleight, C. Y. Jones, and B. H. Toby, J. Solid State Chem. **178**, 285 (2005).
[11] J. P. Doumerc, A. Ammar, A. Wichainchai, M. Pouchard, and P. Hagenmuller, J. Phys. Chem. Solids **48**, 37 (1987).
[12] O. Kovalev, *Representations of the Crystallographic Space Groups* (Gordon and Breach, New York, 1993).
[13] P. G. Radaelli and L. C. Chapon, Phys. Rev. B **76**, 054428 (2007).
[14] A. Munoz, J. A. Alonso, M. J. Martinez-Lope, M. T. Casais, J. L. Martinez, and M. T. Fernandez-Diaz, Phys. Rev. B **62**, 9498 (2000).
[15] T. Okuda, Y. Beppu, Y. Fujii, T. Onoe, N. Terada, and S. Miyasaka, Phys. Rev. B **77**, 134423 (2008).
[16] A. Maignan, C. Martin, R. Frésard, V. Eyert, E. Guilmeau, S. Hébert, and M. Poienar, J. Mater. Chem. (to be published).
[17] J. B. Goodenough, Phys. Rev. **117**, 1442 (1960).
[18] F. Ye, J. A. Fernandez-Baca, R. S. Fishman, Y. Ren, H. J. Kang, Y. Qiu, and T. Kimura, Phys. Rev. Lett. **99**, 157201 (2007).
[19] F. Ye, Y. Ren, Q. Huang, J. A. Fernandez-Baca, P. Dai, J. W. Lynn, and T. Kimura, Phys. Rev. B **73**, 220404(R) (2006).
[20] K. Kimura, H. Nakamura, K. Ohgushi, and T. Kimura, Phys. Rev. B **78**, 140401(R) (2008).
[21] T. H. Arima, J. Phys. Soc. Jpn. **76**, 073702 (2007).